Interactions between nanofibers in fiber-surfactant suspensions: Theory of corresponding distances

Interactions between Nanofibers in Fiber-Surfactant Suspensions: Theory of Corresponding Distances

Dirk Müter* and Henry Bock
Department of Chemical Engineering, Heriot-Watt University, Edinburgh, EH14 4AS Scotland, United Kingdom
(Received 9 August 2013; published 24 March 2014)

We present the theory of corresponding distances for interactions mediated by soft nanostructures in fibrous materials. Based on the fundamental understanding of the mechanism that determines the internal structure of the soft component, our theory allows us to predict the entire force field mediated by the soft component for any angle and distance between the fibers from a single simulation or a single experiment. This replaces hundreds of simulations by just one which enables the routine computation of complete fiber-soft-fiber force fields by high-level methods, such as atomistic simulations, and thereby amounts to a true step advancement for soft nanotechnology.

DOI: 10.1103/PhysRevLett.112.128301 PACS numbers: 82.70.Uv, 05.10.-a, 62.23.St

Fibrous nanoscale building blocks such as carbon nanotubes [1], nanowires [2,3], nanocellulose [4], and cellulose nanocrystals [5] have been of immense interest to the scientific community for more than two decades now, yet they do not cease to inspire new concepts for materials design and engineering [6,7]. However, two major problems impede their widespread use. First, it is largely impossible to produce stable high volume fraction suspensions [8,9] of fibrous nanoparticles. Second, because these nanofibers are usually short [10], they have to be linked together to transfer their individual unique properties to a macroscopic material.

Soft nanostructures based on polymers or self-assembled surfactants can be used to achieve this. While surfactants are commonly used to successfully disperse nanoparticles, in the case of nanofibers such as carbon nanotubes, this is very challenging [8,9,11–14]. Interestingly, at lower bulk concentrations, surfactants can also mediate an attractive force between the tubes that binds them together [15]. Thus, a network of carbon nanotubes could, in principle, be stabilized by these adsorbed surfactant aggregates. This example and the lack of success in dispersing and individualizing carbon nanotubes and cellulose nanocrystals prove that the required understanding is still missing.

What is needed is the fiber-fiber force field that is mediated by the soft component which is accessible through computer simulation [16,17] and, in principle, experimentally. The key problem is that the relevant systems are quite large, their evolution often slow, and the fiber-soft-fiber interaction depends on several parameters, e.g., the distance between the tubes d and their mutual angle α in the case of carbon nanotubes. This makes calculation and also measurement of the entire force field prohibitively expensive.

Here, we present a theory of corresponding distances. It is based on the mechanisms controlling the internal structure of the soft component and describes the distance and angle dependence. This reduces the number of dimensions of the force field that need to be studied directly via simulation by two. This not only enhances our understanding but also dramatically improves the efficiency with which these systems can be studied. As shown for carbon nanotubes, the entire force field can now be obtained from a single simulation. Moreover, the theory also allows the experimental determination of the entire force field—a single fiber-fiber force curve would be sufficient.

To demonstrate the approach, we use dissipative particle dynamics simulations [18] of soft nanostructures self-assembled by surfactant molecules on crossing carbon nanotubes. The surfactants are represented by a bead-spring model and comprise five hydrophilic and five hydrophobic beads [19]. The nanotubes are modeled as smooth rigid cylinders due to their high stiffness. For interactions between the hydrophobic beads, the well-known Lennnard-Jones (LJ) potential with potential depth ϵ and particle diameter σ is employed. For interactions between the hydrophobic beads and the nanotubes, the LJ potential is scaled by a factor of 2.5 and moved to the tube surface. All other interactions are purely repulsive and represented by a truncated LJ potential. The temperature is set to $0.7\epsilon/k_B$. After an initial equilibration phase of 3×10^7 time steps, 2×10^7 time steps were used for statistical averaging. The bulk surfactant concentration is approximately 0.3 times the critical micellar concentration [20]. At this low concentration, the surfactant molecules adsorb predominantly onto the crossing between the nanotubes, where they self-assemble into a central aggregate. The central aggregate engulfs both nanotubes at this position (Fig. 1).

Two important mechanical quantities need to be determined in these systems: $F_z(\alpha, d)$, the surfactant mediated force acting along the shortest distance between the tubes (here, the z axis), and $M_z(\alpha, d)$, the torque trying to rotate the two tubes against each other around the pivot axis (z axis). Both can be calculated from force profiles $F_\lambda(y)$ along the tubes, where $\lambda = x, z$ represents the x and the z

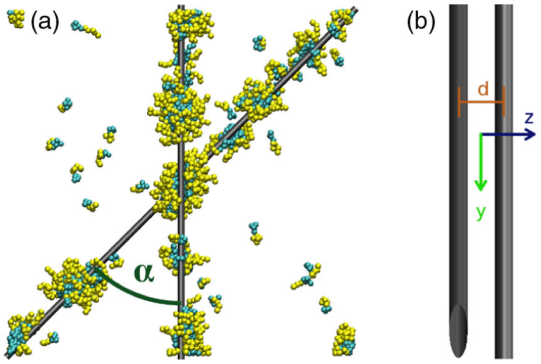

FIG. 1 (color online). Snapshot [21] of the system along (a) the z axis and (b) the x axis.

components, respectively. The force profiles are determined by summation of the force contributions $f_\lambda(i,k)$ from all beads k in all molecules i along the tubes and binning them into small intervals of width Δ. For simplicity, we show this for the horizontal tube in Fig. 3(d):

$$F_\lambda(y) = \left\langle \sum_{i=1}^{N} \sum_{k=1}^{N_{\text{beads}}} f_\lambda(i,k) \right\rangle; \quad y - \frac{\Delta}{2} < y(i,k) < y + \frac{\Delta}{2}, \tag{1}$$

where the angled brackets represent the ensemble average.

As all interactions with the tube are perpendicular to its axis, the y component of the force is always zero. For two different angles between the nanotubes, the force profiles $F_x(y)$ and $F_z(y)$ are shown in Fig. 2. Inspecting the two sets of curves in Fig. 2, one might suggest that the curves for 9° could be derived from the 45° curve by some "stretching" along the abscissa. Such a correspondence does indeed exist.

As the force onto the tubes stems from the adsorbed surfactant beads, the structure of the average force profiles is a consequence of the beads' average spatial arrangement around the tubes. The local density of hydrophobic tail beads shows that the beads form layers around each nanotube close to the crossing where the central aggregate is located (Fig. 3). Such layering is expected due to the liquidlike nature of the soft component. Near the crossing, the overlapping layers form an interference pattern.

Comparing Figs. 3(a) and 3(b), it is evident that the pattern is not fundamentally changed by altering the angle but appears to be "stretched." This is demonstrated in Fig. 3(c), which is a collage of the unmodified upper half of Fig. 3(a) and the stretched lower half of Fig. 3(b). The density patterns match perfectly.

The stretching is actually a slightly more complicated linear transformation that is easily derived in the special case of $d = 0$. Following the analogy of an interference pattern, any

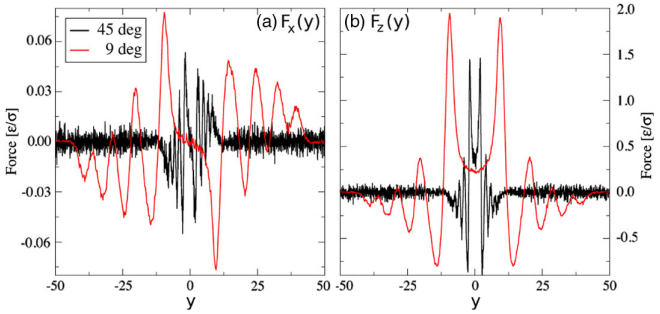

FIG. 2 (color online). Profiles of the x and z components of the surfactant mediated force for two different tube-tube angles as indicated in the figure, at $d = 3.75\sigma$. The 9° curves shows the same features as the 45° curves but appear to be stretched along the abscissa.

point in the $(x, y, z = 0)$ plane between the tubes is fully characterized by its distances to the tubes. For a point located at (y, δ), i.e., at position y along the horizontal tube and a distance δ above its axis [Fig. 3(d)], the distance to the other tube is given as $s(y, \delta, \alpha) = y \sin(\alpha) - \delta \cos(\alpha)$. Consequently, in systems of different angles (α and α'), we find equivalent points in the local density at the same distances to the tubes, i.e., when $\delta = \delta'$ and $s = s'$. This defines the linear transformation

$$y = y' \frac{\sin \alpha'}{\sin \alpha} - \delta \frac{\cos \alpha' - \cos \alpha}{\sin \alpha} \tag{2}$$

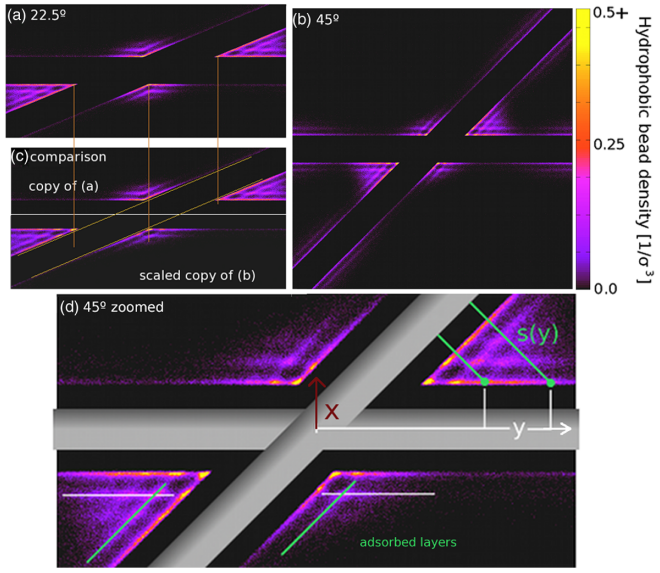

FIG. 3 (color online). Local density of the hydrophobic tail groups around the nanotube crossing $\alpha = 22.5°$ (a) and 45° (b) in the $(x, y, z = 0)$ plane. All plots were produced from a $\Delta z = 0.5\sigma$ thick tile. For better clarity, the separation distance has been set to $d = 0.0\sigma$. The collage in (c) shows that the structures for (a) and (b) can be transformed into each other by a linear transformation (see the text). In the zoomed version in (d), the adsorbed (second) layers are indicated.

which is visualized in Fig. 3(c). In other words, if expressed in terms of δ and s, the local density becomes universal, i.e., independent of the tube-tube angle.

In the general case $d \neq 0$, all points that have the same distance δ to the tube at a position y along its axis lie on the circle (y, δ). The distance $s(y, \delta)$ is now defined as the shortest distance between this circle and the axis of the other tube. This uniquely defines $s(y, \delta)$ and a point $P(y, \delta)$ on the circle that is closest to the other tube

$$s(y,\delta,\alpha,d)=\{[\delta\cos(t)\cos(\alpha)-y\sin(\alpha)]^2+[d-\delta\sin(t)]^2\}^{1/2},$$
$$0=\delta\sin(t)\cos(t)\sin^2(\alpha)+y\sin(t)\cos(\alpha)\sin(\alpha)$$
$$-d\cos(t), \quad (3)$$

where t stems from the parametric representation of the circle.

This correspondence in structure leads to a correspondence in function because the average tube-surfactant forces depend only on the tube-bead interaction potential and the bead density. Since the nanotubes are small, the bead-nanotube interaction is relatively short ranged and thus dominated by the first layer. Accordingly, we assume in all cases that the forces originate solely from the first layer and drop $\delta = \delta^{\text{first}}$. This implies that $F(y, \alpha)$ can be mapped onto $F(y', \alpha')$ via Eq. (3), i.e., $F(y, \alpha) = F(y', \alpha')$ if $s(y, \alpha) = s'(y', \alpha')$.

The mapping is tested by plotting the force components F_x and F_z over $s(y)$ instead of y (Fig. 4). The oscillations in both pairs of curves coincide. However, their amplitudes are not identical. This is expected because at the same s, the total force is expected to have the same magnitude, but it points in slightly different directions in the two cases, as we will show below.

The magnitude of the total force $F(s) = \sqrt{F_x^2(s) + F_z^2(s)}$ is shown in Fig. 5(a). The sign is, of course, lost in this operation, which we alleviate by multiplying $F(s)$ with (-1) whenever $F_x(s)$ and $F_z(s)$ are negative. All curves in Fig. 5(a), including the case of parallel tubes, coincide nearly perfectly. The very small deviations at very small and very large s stem from expected reduced symmetry very close to the crossing (see below) and slight deviations from perfect scalability of the size of the central aggregate, respectively. This proves that the profile of the magnitude of the surfactant mediated force $F(s)$ can be correctly mapped from one system to any other and accordingly that $F(s)$ is indeed independent of α and d.

To predict the force components $F_x(s)$ and $F_z(s)$, we also need to predict the direction of the total force $\mathbf{F}(s)$. The force between a bead and a tube always acts perpendicular to the tube axis. For the horizontal tube (in Fig. 3), this means that the force cannot have a y component. For the $d = 0$ case, it also cannot have a z component (perpendicular to the image plane) due to the mirror symmetry with respect to the $(x, y, z = 0)$ plane. In the general case $d \neq 0$, $\mathbf{F}(s)$ acts along the shortest distance between point $P(s)$ and the horizontal tube. Thus, the unit vector of $\mathbf{F}(s)$ is obtained as $\hat{F} = \mathbf{F}(s)/\|\mathbf{F}(s)\| = [\cos(t), 0, \sin(t)]$, where $t = t(s)$ is given by Eq. (3). It needs to be noted that $P(y)$ was derived by analogy to the $d = 0$ case. This is plausible, as $P(y)$ is the point in the first-layer circle that is under the strongest confinement. Although the symmetry in structure near $P(y)$ will be reduced compared to the $d = 0$ case, local deviations should be relevant only very near the crossing. Comparing the direction of the force as predicted by the theory and in the simulation results [Fig. 5(b)], it is striking how well both components of the force unit vector match. Deviations are observed only where the force is small, and the simulation results therefore carry a large relative error. For all tube-tube angles, $\mathbf{F}(s)$ points in the z direction at the crossing $[y(s) = 0]$ and then turns into the x direction as one moves along the tube and s goes to infinity. The exact way this happens depends on α and d, which explains the difference in amplitudes in Fig. 4.

The results in Fig. 5 compellingly demonstrate that the magnitude of the force F_s can be mapped between all angles α and tube-tube separation distances d and that the direction of $\mathbf{F}(s)$ can be correctly predicted. This means

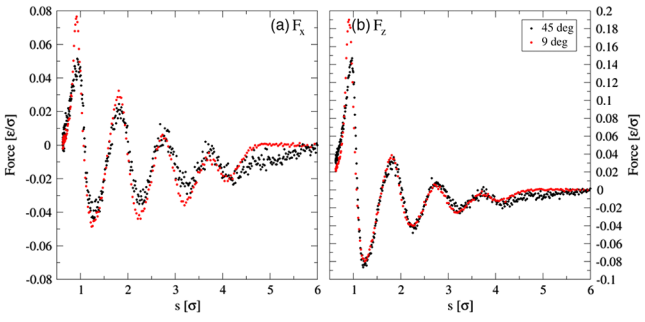

FIG. 4 (color online). The same force profiles as in Fig. 2 but plotted against the distance $s(y)$ indicated in Fig. 3(d). The locations of the oscillations match perfectly.

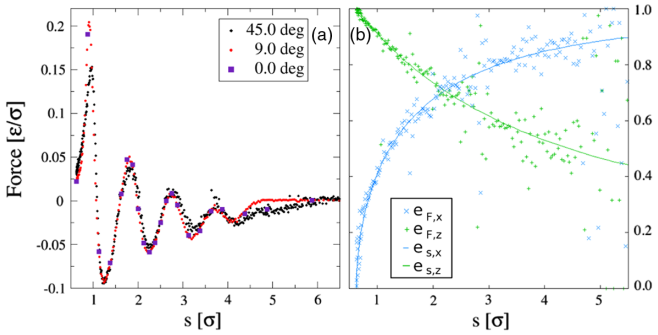

FIG. 5 (color online). (a) The signed magnitude of the force vector $\mathbf{F}(s)$ calculated from the force profiles in Figs. 2 and 4 and from the parallel case is shown. (b) The x and z components of the unit vector of the force from simulations (symbols) and independently predicted by the theory (solid lines). The excellent agreement strongly supports the theory.

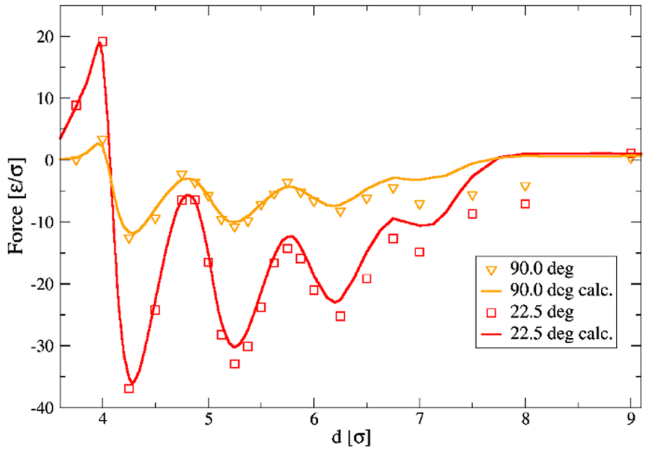

FIG. 6 (color online). The z component exerted by the entire central aggregate onto the tubes as a function of separation distances calculated from 22 individual simulations for each angle [16] and predicted from a single simulation of the system $(\alpha^*, d^*) = (9°, 3.75\sigma)$ using our theory of corresponding distances. Predicting these two curves offers a much higher resolution and is about 50 times more efficient.

that the surfactant mediated forces for any (α, d) can be predicted from a single simulation.

We will demonstrate this by comparing the z component of the cumulative force exerted by the entire central aggregate onto the tubes obtained previously from individual simulations [16,17] with predictions derived from a single simulation at $(\alpha^*, d^*) = (9°, 3.75\sigma)$. The distance d^* must be smaller or equal to any d for which $F_z(\alpha, d)$ is to be predicted. The angle α^* must be larger than zero but is otherwise arbitrary. However, it is advisable to use small angles because of the higher s resolution and better statistics. The predicted force is given by

$$F_z(\alpha, d) = 2 \sum_{s=s(y=0)}^{\infty} \hat{F}_z(s, \alpha, d) F(s) \Delta, \tag{4}$$

where the master curve $F(s)$ is obtained from the simulation at $(\alpha^*, d^*) = (9°, 3.75\sigma)$, while $\hat{F}_z(s, \alpha, d)$ is predicted by the theory of corresponding distances. The predictions in Fig. 6 are in excellent agreement with the points obtained from the individual simulations for most of the d range. Deviations are found only at high separation distances which are due to the aforementioned slight nonscalability of the size of the central aggregate [Fig. 5(a)]. The agreement is truly impressive considering that only one simulation is needed to predict the entire force field $F_z(\alpha, d)$ at essentially arbitrary resolution.

The theoretical description of two dimensions of the force field by our theory of corresponding distances and the additional increase in resolution amount to a tremendous efficiency increase of more than 3 orders of magnitude. Where thousands of individual simulations were required, we now need only one.

A key strength of the theory is that it is not limited to the carbon nanotube-surfactant system studied here (see the Supplemental Material [22]). It is applicable to any fibrous material in which a force between the fibers is mediated by a soft component. The approach is also not limited to any specific simulation technique; it enables the use of more demanding higher-level methods, such as atomistic simulations. Moreover, it is applicable to experiments as well. Here, $\mathbf{F}^{\mathrm{exp}}(s)$ is not usually directly accessible but $F_z(\alpha, d)$ is. This has already been demonstrated for unsolvated tubes [23]. Using Eq. (4), $\mathbf{F}^{\mathrm{exp}}(s)$ can be obtained from $F_z^{\mathrm{exp}}(\alpha = \alpha^*, d)$ measured at any α^*. Although it might be very challenging to measure the parallel case $\alpha = 0$, it is particularly interesting because here s is independent of y, i.e., $s = d - \delta^{\mathrm{first}}$ and $F_x^{\mathrm{exp}}(\alpha = 0, d) = 0$, which means that $F^{\mathrm{exp}}(s)$ is directly accessible via $F_z^{\mathrm{exp}}(\alpha = 0, d) = F^{\mathrm{exp}}[s(d)]$. This adds enormous value to the experimental results because via $\mathbf{F}^{\mathrm{exp}}(s)$, the entire force field $F_z^{\mathrm{exp}}(\alpha, d)$ and $M_z^{\mathrm{exp}}(\alpha, d)$ can be obtained from a single experimental force curve $F_z^{\mathrm{exp}}(\alpha = \alpha^*, d)$.

To conclude, we have analyzed the internal structure of the soft component that mediates interactions between fibers in soft-fiber systems. Based on this understanding, the theory of corresponding distances has been derived, which describes the fiber-fiber distance and angle dependence in fiber-soft-fiber force fields. Our theory reduces the force field dimensions that must be determined directly via simulation or experiment by two. The resulting efficiency increase is very large—more than 3 orders of magnitude. This provides the opportunity to obtain fiber-soft-fiber force fields from high-level simulation methods as well as from experiments. The resulting force fields provide understanding and bridge the gap between the molecular scale and the fiber network scale, enabling the simulation of fiber networks with realistic fiber-soft-fiber force fields. We believe our theory offers a step advancement for the rational design of soft nanostructures in fibrous materials.

D. M. is grateful for financial support for this project through the German Science Foundation's (DFG) research stipend MU 3236/1 "Multiscale modeling of surfactant reinforced carbon nanotube networks."

*Present address: Department of Chemistry, University of Copenhagen, Universitetsparken 5, 2100 Copenhagen, Denmark.

[1] R. H. Baughman, A. A. Zakhidov, and W. A. deHeer, Science **297**, 787 (2002).

[2] W. Hällström, M. Lexholm, D. B. Suyatin, G. Hammarin, D. Hessman, L. Samuelson, L. Montelius, M. Kanje, and C. N. Prinz, Nano Lett. **10**, 782 (2010).

[3] S. Roddaro, K. Nilsson, G. Astromskas, L. Samuelson, L.-E. Wernersson, O. Karlström, and A. Wacker, Appl. Phys. Lett. **92**, 253509 (2008).

[4] D. Klemm, F. Kramer, S. Moritz, T. Lindström, M. Ankerfors, D. Gray, and A. Dorris, Angew. Chem., Int. Ed. Engl. **50**, 5438 (2011).
[5] Y. Habibi, L. A. Lucia, and O. J. Rojas, Chem. Rev. **110**, 3479 (2010).
[6] F. M. Blighe, K. Young, J. J. Vilatela, A. H. Windle, I. A. Kinloch, L. Deng, R. J. Young, and J. N. Coleman, Adv. Funct. Mater. **21**, 364 (2011).
[7] W. Cheung, P. L. Chiu, R. R. Parajuli, Y. Ma, S. R. Ali, and H. He, J. Mater. Chem. **19**, 6465 (2009).
[8] M. S. P. Shaffer, X. Fan, and A. H. Windle, Carbon **36**, 1603 (1998).
[9] V. C. Moore, M. S. Strano, E. H. Haroz, R. H. Hauge, and R. E. Smalley, Nano Lett. **3**, 1379 (2003).
[10] X. Wang, Q. Li, J. Xie, Z. Jin, J. Wang, Y. Li, K. Jiang, and S. Fan, Nano Lett. **9**, 3137 (2009).
[11] J. F. Cardenas and A. Gromov, Nanotechnology **20**, 465703 (2009).
[12] P. Angelikopoulos, A. Gromoy, A. Leen, O. Nerushev, H. Bock, and E. E. B. Campbell, J. Phys. Chem. C **114**, 2 (2010).
[13] P. Angelikopoulos and H. Bock, Phys. Chem. Chem. Phys. **14**, 9546 (2012).
[14] J. N. Coleman, Adv. Funct. Mater. **19**, 3680 (2009).
[15] P. Angelikopoulos and H. Bock, J. Phys. Chem. B **112**, 13793 (2008).
[16] D. Müter, P. Angelikopoulos, and H. Bock, J. Phys. Chem. B **116**, 14869 (2012).
[17] D. Müter and H. Bock, J. Phys. Chem. B **117**, 5585 (2013).
[18] R. D. Groot and P. B. Warren, J. Chem. Phys. **107**, 4423 (1997).
[19] D. Müter, M. A. Widmann, and H. Bock, J. Phys. Chem. Lett. **4**, 2153 (2013).
[20] P. Angelikopoulos and H. Bock, Langmuir **26**, 899 (2010).
[21] W. Humphrey, A. Dalke, and K. Schalke, J. Mol. Graphics **14**, 33 (1996).
[22] See Supplemental Material at http://link.aps.org/supplemental/10.1103/PhysRevLett.112.128301 for application of the theory for two other systems.
[23] B. Bhushan and X. Ling, Phys. Rev. B **78**, 045429 (2008).